 CMES, vol.37, no.3, pp.243-273, 2008

Scattering of flexural wave in thin plate with multiple holes by using the null-field integral equation approach

Wei-Ming Lee[1], **Jeng-Tzong Chen**[2,3]

Abstract: In this paper, a semi-analytical approach is proposed to solve the scattering problem of flexural waves and to determine dynamic moment concentration factors (DMCFs) in an infinite thin plate with multiple circular holes. The null-field integral formulation is employed in conjunction with degenerate kernels, tensor transformation and Fourier series. In the proposed direct formulation, all dynamic kernels of plate are expanded into degenerate forms and further the rotated degenerate kernels have been derived for the general exterior problem. By uniformly collocating points on the real boundary, a linear algebraic system is constructed. The results of dynamic moment concentration factors for the plate with one hole are compared with the analytical solution to verify the validity of the proposed method. For the cases of small wave number, the quasi-static results of a plate with one or multiple circular holes are compared with the static data of finite element method (FEM) using ABAQUS. Numerical results indicate that the DMCF of two holes is apparently larger than that of one hole when two holes are close to each other. Fictitious frequency appeared in the external problem can be suppressed by using the more number of Fourier series terms. The effect of distance between the centers of holes on dynamic moment concentration factors is also investigated by using the proposed method.

Keyword: scattering, flexural wave, dynamic moment concentration, biHelmholtz equation, null-field boundary integral equation, degenerate kernel, Fourier series

1 Introduction

Thin plates with multiple circular holes are widely used in engineering structures, e.g. missiles, aircraft, etc., either to reduce the weight of the whole structure or to increase the range of inspection. Geometric discontinuities due to these holes

[1] Department of Mechanical Engineering, China Institute of Technology, Taipei, Taiwan
[2] Department of Harbor and River Engineering, National Taiwan Ocean University, Keelung, Taiwan
[3] Corresponding author. jtchen@mail.ntou.edu.tw

result in the stress concentration, which reduce the load carrying capacity. The deformation and corresponding stresses produced by the dynamic force are propagated through the structure in the way of waves. At the irregular interface of different media, stress wave reflects in all directions; this phenomenon is the scattering. It turns out that the scattering of the stress wave results in the dynamic stress concentration [Pao and Chao (1972)].

Nishimura and Jimbo [Nishimura and Jimbo (1955)] were two of the early investigators for the analytical study of the dynamic stress concentration and they determined the stresses in the vicinity of a spherical inclusion in the elastic solid under a harmonic force. Pao [Pao (1962)] studied the scattering of flexural waves and dynamic stress concentrations around a circular hole, and proposed an analytical solution. Since then, most research work has focused on the scattering of elastic wave and the resulted dynamic stress concentration and has led to a rapid development of analytical or numerical approach such as the method of wave function expansion, complex variable method, boundary integral equation method and boundary element method [Pao and Chao (1972)].

Kung [Kung (1964)] studied dynamic stress concentrations resulting from the scattering of flexural waves on the thin plate with one circular hole and gave the calculations of moment and shear forces as a function of frequency. Liu *et al*. [Lin, Ga and Tao (1982)] extended the complex variable function approach for statics to the case of dynamic loading. The dynamic stress concentration factors were given for circular and elliptical cavities in an infinite plane by incident plane compressional waves. By using the flux conservation relation and optical theorem, Norris and Vemula [Norris and Vemula (1995)] considered the scattering of flexural waves by circular inclusions with different plate properties and obtained numerical results. The complex variable function approach and conformal mapping technique were employed to solve diffraction problem of flexural waves by two cutouts [Hu, Ma and Huang (1998)] and dynamic concentration factors of plates with two circular holes were presented under various boundary conditions. Squire and Dixon [Squire and Dixon (2000)] applied the wave function expansion method to study the scattering properties of a single coated cylindrical anomaly located in a thin plate on which flexural waves propagate. Gao *et al*. [Gao, Wang and Ma (2001)] dealt with theoretical and numerical analysis of scattering of elastic wave and dynamic stress concentrations in an infinite plate with a circular hole using the boundary element method. Hayir and Bakirtas [Hayir and Bakirtas (2004)] applied the image method to analyze the scattering and dynamic stress concentrations of elastic waves in plates with a circular hole subject to the plane harmonic SH wave. Gao *et al*. [Gao, Wang, Zhang and Ma (2005)] studied the scattering of flexural waves and calculated the dynamic stress concentration in the thin plate with the cutout

by using the dual reciprocity boundary element method. Hu *et al*. [Hu, Fang and Huang (2007)] applied the image method and the wave function expansion method to study the multiple scattering of flexural waves in semi-infinite plates with a circular cutout. Recently, one monograph is devoted to discussing the multiple scattering in acoustics, electromagnetism, seismology and hydrodynamics [Martin (2006)].

From literature reviews stated previously, few papers except Hu *et al*. [Hu, Ma and Huang (1998)] have been published to date reporting the scattering of flexural wave in plate with more than one cutout. Furthermore, as Kobayashi and Nishimura [Kobayashi and Nishimura (1981)] pointed out that the integral equation method seems to be most effective for two-dimensional steady-state flexural wave [Chen, Fu and Zhang (2007); Chandrasekhar, Rao (2007); Chandrasekhar (2008)]. In the paper, the boundary integral method is devoted to solving the multiple scattering of flexural wave and dynamic stress concentrations in plate with multiple circular holes.

It is noted that improper integrals on the boundary should be handled particularly when the BEM or BIEM is used. In the past, many researchers proposed several regularization techniques to deal with the singularity and hypersingularity. The determination of the Cauchy principal value (CPV) and the Hadamard principal value (HPV) in the singular and hypersingular integrals are critical issues in BEM/BIEM [Chen and Hong (1999); Tanaka, Sladek and Sladek (1994)]. For the plate problem, it is more difficult to calculate the principal values since the kernels are involved with transcendental functions and their higher-order gradients. Readers can consult with the review article by Beskos [Beskos (1997)]. In this paper, instead of using the previous concepts, the kernel function is recast into the degenerate kernel which is expanded into a series form on each side (interior and exterior) of the boundary by employing the addition theorem since the double layer potential is discontinuous across the boundary. In reality, addition theorems are expansion formulae for the special functions (e.g. Bessel function, spherical harmonics, etc.) in a selected coordinate system [Gradshteyn and Ryzhik (1996)]. Therefore, degenerate kernel, namely separable kernel, is a vital tool to study the perforated plate. Based on the direct boundary integral formulation, Chen *et al.* [Chen, Shen and Chen (2006a); Chen, Hsiao and Leu (2006b)] recently proposed null-field integral equations in conjunction with degenerate kernels and Fourier series to solve boundary value problems with circular boundaries. By introducing the degenerate (separable) kernel, BIE involves nothing more than the linear algebra. Some applications were done in the plate problems [Chen, Hsiao and Leu (2006b)] and the derivation of anti-plane dynamic Green's function [Chen and Ke (2008)]. The introduction of degenerate kernel in companion with Fourier series was proved to yield the exponential convergence [Kress (1989)] instead of the linear algebraic convergence in

BEM.

This paper presents a semi-analytical approach to solve scattering of flexural waves and dynamic moment concentration factors in a thin plate with multiple circular holes. A linear algebraic system will be constructed by taking finite terms of Fourier series after uniformly collocating points on the boundary. After determining the Fourier coefficients of unknown boundary densities, the displacement and corresponding section force produced by the incident flexural wave are determined by using the boundary integral equations for the domain point. For the plate problem, the slope (bending angle) and moment in the normal and tangential directions for the multiply-connected domain problem are determined with care under the adaptive observer system. Therefore, the operator of transformation matrix for the slope and moment is adopted to deal with this problem. Finally, the obtained result for an infinite plate with one circular hole is compared with the analytical solution [Kung (1964)] to verify the validity of the present method. For the cases of small wave number, the results for more than one hole will be compared with those of FEM using ABAQUS to demonstrate the generality of the proposed method. Finally, the effect of central distance between holes on dynamic moment concentration factors is also investigated by the proposed method.

2 Problem statement and boundary integral formulation

2.1 Problem statement

The governing equation of the flexural wave for a uniform infinite thin plate with randomly distributed circular holes as shown in Figure 1 is written as follows:

$$\nabla^4 u(x) = k^4 u(x), \quad x \in \Omega \tag{1}$$

where ∇^4 is the biharmonic operator, u is the out-of-plane elastic displacement, $k^4 = \omega^2 \rho_0 h/D$, k (2π/wave length) is the wave number of elastic wave, ω is the circular frequency, ρ_0 is the volume density, $D = Eh^3/12(1-\mu^2)$ is the flexural rigidity, E denotes the Young's modulus, μ is the Poisson ratio, h is the plate thickness and Ω is the domain of the thin plate..

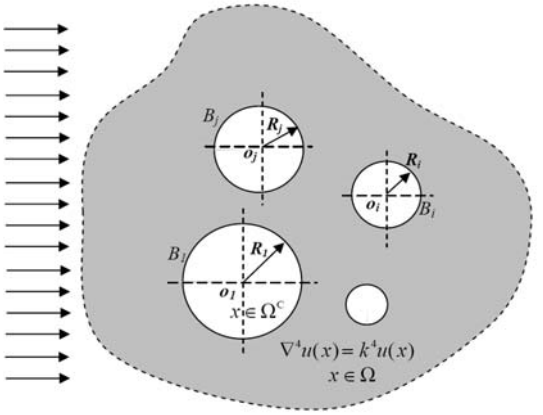

Figure 1: Problem statement for an infinite plate with multiple circular holes subject to an incident flexural wave

2.2 Boundary integral equation for the collocation point in the domain

The integral representation for the plate problem can be derived from the Rayleigh-Green identity [Kitahara (1985)] as follows:

$$u(x) = \int_B U(s,x)v(s)dB(s) - \int_B \Theta(s,x)m(s)dB(s) + \int_B M(s,x)\theta(s)dB(s) - \int_B V(s,x)u(s)dB(s), \quad x \in \Omega \quad (2)$$

$$\theta(x) = \int_B U_\theta(s,x)v(s)dB(s) - \int_B \Theta_\theta(s,x)m(s)dB(s) + \int_B M_\theta(s,x)\theta(s)dB(s) - \int_B V_\theta(s,x)u(s)dB(s), \quad x \in \Omega \quad (3)$$

$$m(x) = \int_B U_m(s,x)v(s)dB(s) - \int_B \Theta_m(s,x)m(s)dB(s) + \int_B M_m(s,x)\theta(s)dB(s) - \int_B V_m(s,x)u(s)dB(s), \quad x \in \Omega \quad (4)$$

$$v(x) = \int_B U_v(s,x)v(s)dB(s) - \int_B \Theta_v(s,x)m(s)dB(s) + \int_B M_v(s,x)\theta(s)dB(s) - \int_B V_v(s,x)u(s)dB(s), \quad x \in \Omega \quad (5)$$

where B is the boundary of the domain Ω; $u(x)$, $\theta(x)$, $m(x)$ and $v(x)$ are the displacement, slope, moment and shear force; $U(s,x)$, $\Theta(s,x)$, $M(s,x)$, $V(s,x)$, $U_\theta(s,x)$, $\Theta_\theta(s,x)$, $M_\theta(s,x)$, $V_\theta(s,x)$, $U_m(s,x)$, $\Theta_m(s,x)$, $M_m(s,x)$, $V_m(s,x)$, $U_v(s,x)$, $\Theta_v(s,x)$, $M_v(s,x)$ and $V_v(s,x)$ are kernel functions; s and x mean the source and field points, respectively. It is noted that the null field points do not include the boundary in the conventional BIEM. But it can be done when the kernel functions in Eqs.(2)-(5) are expanded to degenerate kernels, which will be described in section 2.4. The kernel function $U(s,x)$ in Eq.(2) is the fundamental solution which satisfies

$$\nabla^4 U(s,x) - k^4 U(s,x) = \delta(s-x) \quad (6)$$

where $\delta(s-x)$ is the Dirac-delta function, respectively. Considering the two singular solutions ($Y_0(kr)$ and $K_0(kr)$, which are the zeroth-order of the second-kind Bessel and modified Bessel functions, respectively) [Hutchinson (1991)] and one regular solution ($J_0(kr)$ is the zeroth-order of the first-kind Bessel) in the fundamental solution, we have the complex-valued kernel,

$$U(s,x) = \frac{1}{8k^2 D}\left[Y_0(kr) - iJ_0(kr) + \frac{2}{\pi}K_0(kr)\right], \quad (7)$$

where $r \equiv |s-x|$ and $i^2 = -1$, which ensures the outgoing wave in companion with $e^{-i\omega t}$. The other three kernels, $\Theta(s,x)$, $M(s,x)$ and $V(s,x)$, in Eq.(2) can be obtained by applying the following slope, moment and effective shear operators defined by

$$K_\Theta = \frac{\partial(\cdot)}{\partial n} \quad (8)$$

$$K_M = -D\left[\nu\nabla^2(\cdot) + (1-\nu)\frac{\partial^2(\cdot)}{\partial n^2}\right] \quad (9)$$

$$K_V = -D\left[\frac{\partial}{\partial n}\nabla^2(\cdot) + (1-\nu)\frac{\partial}{\partial t}\left(\frac{\partial}{\partial n}\left(\frac{\partial}{\partial t}(\cdot)\right)\right)\right] \quad (10)$$

to the kernel $U(s,x)$ with respect to the source point, where $\partial/\partial n$ and $\partial/\partial t$ are the normal and tangential derivatives, respectively; ∇^2 means the Laplacian operator.

In the polar coordinate of (R,θ), the normal and tangential derivatives can be expressed by $\partial/\partial R$ and $(1/R)\partial/\partial\theta$, respectively, and then the three kernel functions can be expressed as:

$$\Theta(s,x) = K_{\Theta,s}(U(s,x)) = \frac{\partial U(s,x)}{\partial R} \tag{11}$$

$$M(s,x) = K_{M,s}(U(s,x)) = -D\left[\nu\nabla_s^2 U(s,x) + (1-\nu)\frac{\partial^2 U(s,x)}{\partial R^2}\right] \tag{12}$$

$$\begin{aligned} V(s,x) &= K_{V,s}(U(s,x)) \\ &= -D\left[\frac{\partial}{\partial R}\left(\nabla_s^2 U(s,x)\right) + (1-\nu)\left(\frac{1}{R}\right)\frac{\partial}{\partial\theta}\left(\frac{\partial}{\partial R}\left(\frac{1}{R}\frac{\partial U(s,x)}{\partial\theta}\right)\right)\right] \end{aligned} \tag{13}$$

The expressions for $\theta(x)$, $m(x)$ and $v(x)$ in Eqs.(3)-(5), which can be obtained by applying the operators in Eqs.(8)-(10) to $u(x)$ in Eq. (2) with respect to the field point $x(\rho,\phi)$, are

$$\theta(x) = K_{\Theta,x}(u(x)) = \frac{\partial u(x)}{\partial\rho} \tag{14}$$

$$m(x) = K_{M,x}(u(x)) = -D\left[\nu\nabla^2 u(x) + (1-\nu)\frac{\partial^2 u(x)}{\partial\rho^2}\right] \tag{15}$$

$$\begin{aligned} v(x) &= K_{V,x}(u(x)) \\ &= -D\left[\frac{\partial}{\partial\rho}\left(\nabla_s^2 u(x)\right) + (1-\nu)\left(\frac{1}{\rho}\right)\frac{\partial}{\partial\phi}\left[\frac{\partial}{\partial\rho}\left(\frac{1}{\rho}\frac{\partial u(x)}{\partial\phi}\right)\right]\right]. \end{aligned} \tag{16}$$

By this way, the kernel functions $U_\theta(s,x)$, $\Theta_\theta(s,x)$, $M_\theta(s,x)$, $V_\theta(s,x)$, $U_m(s,x)$, $\Theta_m s,x)$, $M_m(s,x)$, $V_m(s,x)$, $U_v(s,x)$, $\Theta_v(s,x)$, $M_v(s,x)$ and $V_v(s,x)$ can be obtained by applying the operators in Eqs.(8)-(10) to $U(s,x)$, $\Theta(s,x)$, $M(s,x)$ and $V(s,x)$ with respect to the field point $x(\rho,\phi)$.

2.3 Null-field integral equations

The null-field integral equations derived by collocating the field point outside the domain (including the boundary point if exterior degenerate kernels are properly adopted) are shown as follows:

$$\begin{aligned} 0 = \int_B U(s,x)v(s)dB(s) - \int_B \Theta(s,x)m(s)dB(s) + \int_B M(s,x)\theta(s)dB(s) \\ - \int_B V(s,x)u(s)dB(s), \quad x \in \Omega^C \cup B, \end{aligned} \tag{17}$$

$$0=\int_B U_\theta(s,x)v(s)dB(s)-\int_B \Theta_\theta(s,x)m(s)dB(s)+\int_B M_\theta(s,x)\theta(s)dB(s) -\int_B V_\theta(s,x)u(s)dB(s),\quad x\in\Omega^C\cup B, \quad (18)$$

$$0=\int_B U_m(s,x)v(s)dB(s)-\int_B \Theta_m(s,x)m(s)dB(s)+\int_B M_m(s,x)\theta(s)dB(s) -\int_B V_m(s,x)u(s)dB(s),\quad x\in\Omega^C\cup B, \quad (19)$$

$$0=\int_B U_v(s,x)v(s)dB(s)-\int_B \Theta_v(s,x)m(s)dB(s)+\int_B M_v(s,x)\theta(s)dB(s) -\int_B V_v(s,x)u(s)dB(s),\quad x\in\Omega^C\cup B, \quad (20)$$

where Ω^C is the complementary domain of Ω. Once kernel functions are expressed in proper degenerate forms, which will be described in the next subsection, the collocation points can be exactly located on the real boundary, that is $x\in\Omega^C\cup B$. Since the four equations of Eqs.(17)-(20) in the plate formulation are provided, there are 6 (C_2^4) options for choosing any two equations to solve the problems.

2.4 Degenerate kernels and Fourier series for boundary densities

In the plane polar coordinate, the field point and source point can be expressed as (ρ,ϕ) and (R,θ), respectively. By applying the addition theorem [Gradshteyn and Ryzhik (1996)] to Eq. (7), the degenerate form for the kernel function $U(s,x)$ can be expressed in the series form as follows

$$U:\begin{cases} U^I(s,x)= & \frac{1}{8k^2D}\sum\limits_{m=0}^{\infty}\varepsilon_m\{J_m(k\rho)[Y_m(kR)-iJ_m(kR)] \\ & +\frac{2}{\pi}I_m(k\rho)K_m(kR)\}\cos[m(\theta-\phi)], \quad \rho<R \\ U^E(s,x)= & \frac{1}{8k^2D}\sum\limits_{m=0}^{\infty}\varepsilon_m\{J_m(kR)[Y_m(k\rho)-iJ_m(k\rho)] \\ & +\frac{2}{\pi}I_m(kR)K_m(k\rho)\}\cos[m(\theta-\phi)], \quad \rho\geq R \end{cases} \quad (21)$$

where ε_m is the Neumann factor (ε_m=1, m=0; ε_m=2, m=1,2,$\cdots,\infty$) and the superscripts "I" and "E" denote the interior and exterior cases for $U(s,x)$ degenerate kernels to distinguish $\rho<R$ and $\rho>R$, respectively as shown in Figure 2. The

degenerate kernels $\Theta(s,x)$, $M(s,x)$ and $V(s,x)$ in the null-field boundary integral equations can be obtained by applying the operators of Eqs.(8)-(10) to the degenerate kernel $U(s,x)$, given by Eq.(21), with respect to the source point s. The other degenerate kernels $U_\theta(s,x)$, $\Theta_\theta(s,x)$, $M_\theta(s,x)$, $V_\theta(s,x)$, $U_m(s,x)$, $\Theta_m(s,x)$, $M_m(s,x)$, $V_m(s,x)$, $U_v(s,x)$, $\Theta_v(s,x)$, $M_v(s,x)$ and $V_v(s,x)$ can be obtained by applying the operators of Eqs.(8)-(10) to the degenerate kernel $U(s,x)$, $\Theta(s,x)$, $M(s,x)$ and $V(s,x)$ with respect to the field point x. The expressions of these degenerate kernels are listed in the Appendix I.

In order to fully utilize the geometry of circular boundary, the displacement $u(s)$, slope $\theta(s)$, moment $m(s)$ and shear force $v(s)$ along the circular boundaries in the null-field integral equations are represented by using Fourier series expansion, respectively, as shown below:

$$u(s) = u_{c0} + \sum_{n=1}^{M} (u_{cn}\cos n\theta + u_{sn}\sin n\theta), \quad s \in B, \tag{22}$$

$$\theta(s) = \theta_{c0} + \sum_{n=1}^{M} (\theta_{cn}\cos n\theta + \theta_{sn}\sin n\theta), \quad s \in B, \tag{23}$$

$$m(s) = m_{c0} + \sum_{n=1}^{M} (m_{cn}\cos n\theta + m_{sn}\sin n\theta), \quad s \in B, \tag{24}$$

$$v(s) = v_{c0} + \sum_{n=1}^{M} (v_{cn}\cos n\theta + v_{sn}\sin n\theta), \quad s \in B, \tag{25}$$

where u_{c0}, u_{cn}, u_{sn}, θ_{c0}, θ_{cn}, θ_{sn}, m_{c0}, m_{cn}, m_{sn}, v_{c0}, v_{cn} and v_{sn} are the Fourier coefficients and M is the truncated number of Fourier series terms. The number of terms M in the Fourier series for circular boundaries can be, in general, different for each boundary circle. For simplicity, we used the same number of Fourier terms for each circular boundary. By using degenerate kernels, Fourier series and orthogonal property, all the improper integrals in Eqs.(17)-(20) can be transformed to series sum and then be calculated easily, since the potential across the boundary can be described by using the degenerate kernel with a series form in each side. Successful experiences on Laplace problems [Chen, Shen and Chen (2006a)], Helmholtz problems [Chen ×4 (2007)] and biharmonic problems [Chen, Hsiao and Leu (2006b)] can be found.

3 Adaptive observer system and transformation of tensor components

3.1 Adaptive observer system

For the direct boundary integral equations being frame indifferent (*i.e.* rule of objectivity), the origin of the observer system can be adaptively located on the center

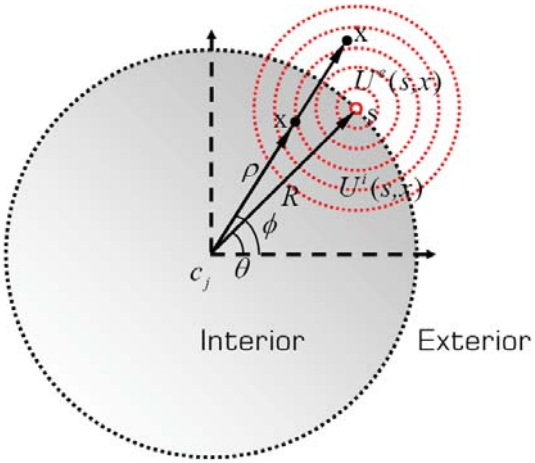

Figure 2: Degenerate kernel for $U(s,x)$

of the corresponding boundary contour under integration. Adaptive observer system is chosen to fully employ the circular property, which takes the full advantage of both Fourier series to represent boundary variables and degenerate-kernel expressions in the polar coordinate. Figure 3 shows the boundary integration for the circular boundaries in the adaptive observer system. The dummy variable in the circular contour integration is only the angle θ. By using the adaptive system, all the boundary integrals can be determined analytically free of calculating principal value.

3.2 Transformation of tensor components

For the slope, moment and effective shear force being calculated in the plate problem, special treatment for the potential gradient or higher-order gradient should be taken care as the source and field points locate on different circular boundaries. As shown in Figure 4, the angle ϕ_i is polar coordinate of the collocation point x_i centered at o_i which locates the center of the circle under integration and the angle ϕ_c is that centered at o_j being the center of the circle on which the collocation point is located. According to the transformation law for the components of tensor, we have

$$\begin{bmatrix}(\cdot)_n\\(\cdot)_t\end{bmatrix} = \begin{bmatrix}\cos(\delta) & \sin(\delta)\\-\sin(\delta) & \cos(\delta)\end{bmatrix}\begin{bmatrix}(\cdot)_r\\(\cdot)_\theta\end{bmatrix} \tag{26}$$

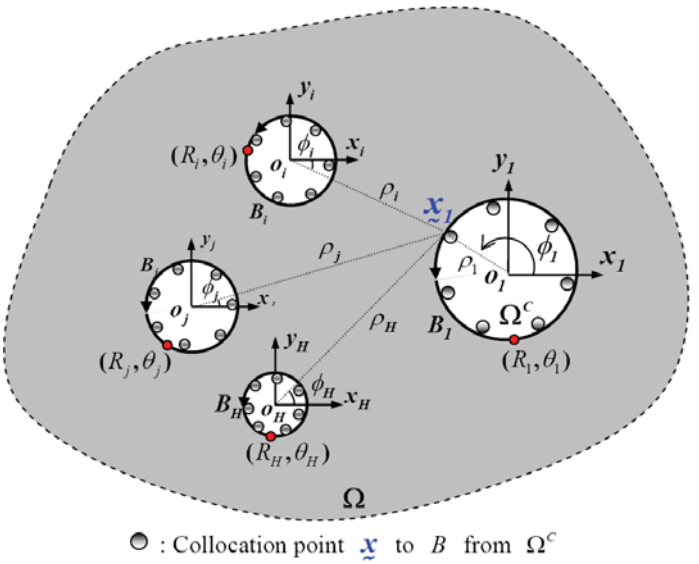

Figure 3: Collocation point and boundary contour integration in the boundary integral equation by using the adaptive observer system

$$\begin{bmatrix}(\cdot)_{nn}\\(\cdot)_{tt}\\(\cdot)_{nt}\end{bmatrix} = \begin{bmatrix}\cos^2(\delta) & \sin^2(\delta) & 2\sin(\delta)\cos(\delta)\\ \sin^2(\delta) & \cos^2(\delta) & -2\sin(\delta)\cos(\delta)\\ -\sin(\delta)\cos(\delta) & \sin(\delta)\cos(\delta) & \cos^2(\delta)-\sin^2(\delta)\end{bmatrix}\begin{bmatrix}(\cdot)_{rr}\\(\cdot)_{\theta\theta}\\(\cdot)_{r\theta}\end{bmatrix}. \quad (27)$$

Based on Eqs. (26) and (27), the general rotated slope, normal bending and tangential bending moment kernels can be obtained by using following operators:

$$K_\Theta^R = \cos(\delta)\frac{\partial(\cdot)}{\partial n} + \sin(\delta)\frac{\partial(\cdot)}{\partial t} \quad (28)$$

$$K_N^R = -D\left\{\left[\nu+(1-\nu)\sin^2(\delta)\right]\nabla^2(\cdot) + \cos(2\delta)(1-\nu)\frac{\partial^2(\cdot)}{\partial n^2} + \sin(2\delta)(1-\nu)\frac{\partial}{\partial n}\left(\frac{\partial(\cdot)}{\partial t}\right)\right\} \quad (29)$$

$$K_T^R = -D\left\{\left[\nu+(1-\nu)\cos^2(\delta)\right]\nabla^2(\cdot) + \cos(2\delta)(\nu-1)\frac{\partial^2(\cdot)}{\partial n^2} - \sin(2\delta)(1-\nu)\frac{\partial}{\partial n}\left(\frac{\partial(\cdot)}{\partial t}\right)\right\} \quad (30)$$

where $\delta = \phi_c - \phi_i$. When the angle ϕ_c equals to the angle ϕ_i or two circles coincide, the angle difference δ equals to zero and Eqs.(28) and (29) are simplified to Eqs.(8) and (9), respectively. The expressions of rotated degenerate kernels, $U_\theta(s,x)$, $\Theta_\theta(s,x)$, $M_\theta(s,x)$, $V_\theta s,x)$, $U_m(s,x)$, $\Theta_m(s,x)$, $M_m(s,x)$, $V_m(s,x)$, $U_t(s,x)$, $\Theta_t(s,x)$, $M_t(s,x)$ and $V_t(s,x)$, can be obtained by applying the operators of Eqs.(28), (29) and (30) to the degenerate kernel $U(s,x)$, $\Theta(s,x)$, $M(s,x)$ and $V(s,x)$ with respect to the field point x and are listed in the Appendix II.

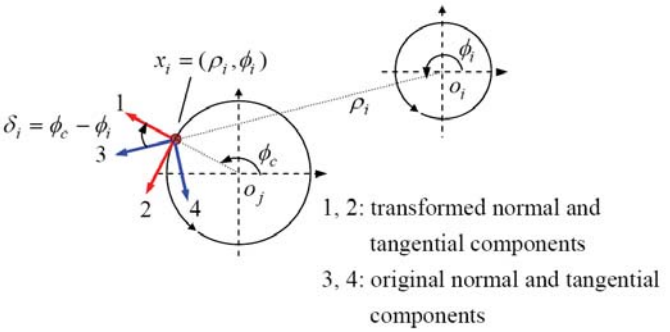

Figure 4: Transformation of tensor components

4 Linear algebraic systems

Consider an infinite plate containing H nonoverlapping circular holes centered at the position vector o_j (j=1, 2, $\cdots$, H), as shown in Fig. 3 in which R_j denotes the radius of the jth circular region, $\underset{\sim}{x}_j$ is the collocation point on the jth circular boundary and B_j is the boundary of the jth circular hole. Kernels of Eqs. (19) and (20) involve higher-order derivatives, which may decrease both the convergence rate and computational efficiency. For the purpose of computational efficiency, Eqs. (17) and (18) are used to analyze the plate problem. By uniformly collocating N (=2M+1) points on each circular boundary in Eqs. (17) and (18), we have

$$0 = \sum_{j=1}^{H} \int_{B_j} \{U(s,x)v(s) - \Theta(s,x)m(s) + M(s,x)\theta(s) - V(s,x)u(s)\}\, dB_j(s), \quad x \in \Omega^C, \quad (31)$$

$$0=\sum_{j=1}^{H}\int_{B_j}\{U_\theta(s,x)v(s)-\Theta_\theta(s,x)m(s)+M_\theta(s,x)\theta(s)-V_\theta(s,x)u(s)\}\,dB_j(s),$$

$$x\in\Omega^C. \quad (32)$$

For the B_j circular boundary integrals, the degenerate kernels of $U(s,x)$, $\Theta(s,x)$, $M(s,x)$, $V(s,x)$, $U_\theta(s,x)$, $\Theta_\theta(s,x)$, $M_\theta(s,x)$ and $V_\theta(s,x)$ are utilized and boundary densities $u(s)$, $\theta(s)$, $m(s)$ and $v(s)$ along the circular boundary are represented by using the Fourier series of Eqs.(22)-(25), respectively. By using the conventional boundary integral equations to solve a problem, the determination of the Cauchy principal value (CPV) and the Hadamard principal value (HPV) for boundary integrals of various kernel functions are inevitable. By using the addition theorem, the kernel functions in our method are expanded in the series form and the boundary integrals can be easily calculated using the series sum free of facing principal values. The selection of interior or exterior degenerate kernel depends on $\rho<R$ or $\rho>R$, respectively, according to the observer system. In the B_j integration, the origin of the observer system is adaptively set to collocate at the center o_j from which the degenerate kernels and Fourier series are described. By using the orthogonal property, a linear algebraic system can be written as follows:

$$\begin{bmatrix} U^{11} & -\Theta^{11} & U^{12} & -\Theta^{12} & \cdots & U^{1H} & -\Theta^{1H} \\ U_\theta^{11} & -\Theta_\theta^{11} & U_\theta^{12} & -\Theta_\theta^{12} & \cdots & U_\theta^{1H} & -\Theta_\theta^{1H} \\ U^{21} & -\Theta^{21} & U^{22} & -\Theta^{22} & \cdots & U^{2H} & -\Theta^{2H} \\ U_\theta^{21} & -\Theta_\theta^{21} & U_\theta^{22} & -\Theta_\theta^{22} & \cdots & U_\theta^{2H} & -\Theta_\theta^{2H} \\ \vdots & \vdots & \vdots & \vdots & \ddots & \vdots & \vdots \\ U^{H1} & -\Theta^{H1} & U_\theta^{H2} & -\Theta^{H2} & \cdots & U^{HH} & -\Theta^{HH} \\ U_\theta^{H1} & -\Theta_\theta^{H1} & U_\theta^{H2} & -\Theta_\theta^{H2} & \cdots & U_\theta^{HH} & -\Theta_\theta^{HH} \end{bmatrix} \begin{Bmatrix} v^1 \\ m^1 \\ v^2 \\ m^2 \\ \vdots \\ v^H \\ m^H \end{Bmatrix}$$

$$= \begin{bmatrix} -M^{11} & V^{11} & -M^{12} & V^{12} & \cdots & -M^{1H} & V^{1H} \\ -M_\theta^{11} & V_\theta^{11} & -M_\theta^{12} & V_\theta^{12} & \cdots & -M_\theta^{1H} & V_\theta^{1H} \\ -M^{21} & V^{21} & -M^{22} & V^{22} & \cdots & -M^{2H} & V^{2H} \\ -M_\theta^{21} & V_\theta^{21} & -M_\theta^{22} & V_\theta^{22} & \cdots & -M_\theta^{2H} & V_\theta^{2H} \\ \vdots & \vdots & \vdots & \vdots & \ddots & \vdots & \vdots \\ -M^{H1} & V^{H1} & -M_\theta^{H2} & V^{H2} & \cdots & -M^{HH} & V^{HH} \\ -M_\theta^{H1} & V_\theta^{H1} & -M_\theta^{H2} & V_\theta^{H2} & \cdots & -M_\theta^{HH} & V_\theta^{HH} \end{bmatrix} \begin{Bmatrix} \theta^1 \\ u^1 \\ \theta^2 \\ u^2 \\ \vdots \\ \theta^H \\ u^H \end{Bmatrix} \quad (33)$$

where H denotes the number of circular boundaries. For brevity, a unified form $[U^{ij}]$ ($i=1,2,3,\cdots,H$ and $j=1,2,3,\cdots,H$) denote the response of $U(s,x)$ kernel at the ith circle point due to the source at the jth circle. Otherwise, the same definition is for $[\Theta^{ij}]$, $[M^{ij}]$, $[V^{ij}]$, $[U_\theta^{ij}]$, $[\Theta_\theta^{ij}]$, $[M_\theta^{ij}]$ and $[V_\theta^{ij}]$ kernels. The explicit

expressions for sub-vectors $[u^i]$, $[\theta^i]$, $[m^i]$ and $[v^i]$ can be described as follows:

$$u^i = \begin{Bmatrix} u^i_{c0} \\ u^i_{c1} \\ u^i_{s1} \\ \vdots \\ u^i_{cM} \\ u^i_{sM} \end{Bmatrix}, \quad \theta^i = \begin{Bmatrix} \theta^i_{c0} \\ \theta^i_{c1} \\ \theta^i_{s1} \\ \vdots \\ \theta^i_{cM} \\ \theta^i_{sM} \end{Bmatrix}, \quad m^i = \begin{Bmatrix} m^i_{c0} \\ m^i_{c1} \\ m^i_{s1} \\ \vdots \\ m^i_{cM} \\ m^i_{sM} \end{Bmatrix}, \quad v^i = \begin{Bmatrix} v^i_{c0} \\ v^i_{c1} \\ v^i_{s1} \\ \vdots \\ v^i_{cM} \\ v^i_{sM} \end{Bmatrix}. \tag{34}$$

The explicit expressions for the sub-matrices of $[U^{ij}]$, $[\Theta^{ij}]$, $[M^{ij}]$, $[V^{ij}]$, $[U^{ij}_\theta]$, $[\Theta^{ij}_\theta]$, $[M^{ij}_\theta]$ and $[V^{ij}_\theta]$ can be written as shown below

$$K^{ij} = \begin{bmatrix} K^{ij}_{0C}(\rho_1,\phi_1) & K^{ij}_{1C}(\rho_1,\phi_1) & K^{ij}_{1S}(\rho_1,\phi_1) & \cdots & K^{ij}_{MS}(\rho_1,\phi_1) \\ K^{ij}_{0C}(\rho_2,\phi_2) & K^{ij}_{1C}(\rho_2,\phi_2) & K^{ij}_{1S}(\rho_2,\phi_2) & \cdots & K^{ij}_{MS}(\rho_2,\phi_2) \\ \vdots & \vdots & \vdots & & \vdots \\ \vdots & \vdots & \vdots & & \vdots \\ K^{ij}_{0C}(\rho_N,\phi_N) & K^{ij}_{1C}(\rho_N,\phi_N) & K^{ij}_{1S}(\rho_N,\phi_N) & \cdots & K^{ij}_{MS}(\rho_N,\phi_N) \end{bmatrix}_{N\times N} \tag{35}$$

where K can be either one of $U(s,x)$, $\Theta(s,x)$, $M(s,x)$, $V(s,x)$, $U_\theta(s,x)$, $\Theta_\theta(s,x)$, $M_\theta(s,x)$ and $V_\theta(s,x)$. The notations ϕ_k and ρ_k $(k = 1,2,3,\cdots,N)$ shown in Fig. 3 are the angle and radius of the k-th collocation point on the i-th circular boundary with respect to the center of the j-th circular boundary (the origin of the observer system) and the element of the sub-matrices can be determined by

$$K^{ij}_{nC}(\rho_k,\phi_k) = \int_0^{2\pi} K(R_j,\theta_j;\rho_k,\phi_k)\,\cos(n\theta_j)\,(R_j d\theta_j), \quad n = 0,1,2,\cdots,M, \tag{36}$$

$$K^{ij}_{nS}(\rho_k,\phi_k) = \int_0^{2\pi} K(R_j,\theta_j;\rho_k,\phi_k)\,\sin(n\theta_j)\,(R_j d\theta_j), \quad n = 1,2,\cdots,M \tag{37}$$

in which the selection of interior or exterior degenerate kernel depends on the position of collocation point with respective to the center of circle under integration as shown in Fig. 3.

5 Dynamic moment concentration factor and techniques for solving scattering problems

Considering an infinite thin plate with multiple holes subject to the incident flexural wave, the boundary conditions of the hole are free. For this scattering problem, it can be decomposed into two parts, (a) incident wave field and (b) radiation field, as shown in Fig. 5. For matching the boundary conditions, the radiation boundary

condition in part (b) is obtained as the minus quantity of incident wave function, *e.g.* $m^R = -m^I; v^R = -v^I$ for the free edge where the superscripts R and I denote radiation and incidence, respectively. By substituting the known radiation boundary conditions, $-m^I$ and $-v^I$, into the left hand side of Eq. (33), the unknown boundary data, u and θ, can be solved. After calculating the displacement, slope, moment and effective shear force along the boundary, the radiation field can be solved by employing the boundary integral equation for the domain point of Eqs. (2)-(5). The scattering field is determined by superimposing radiation field and incident field. The tangential bending moment $M_t(x)$ can be determined by applying the operator in Eq.(30) to Eq.(2) with respective to the field point.

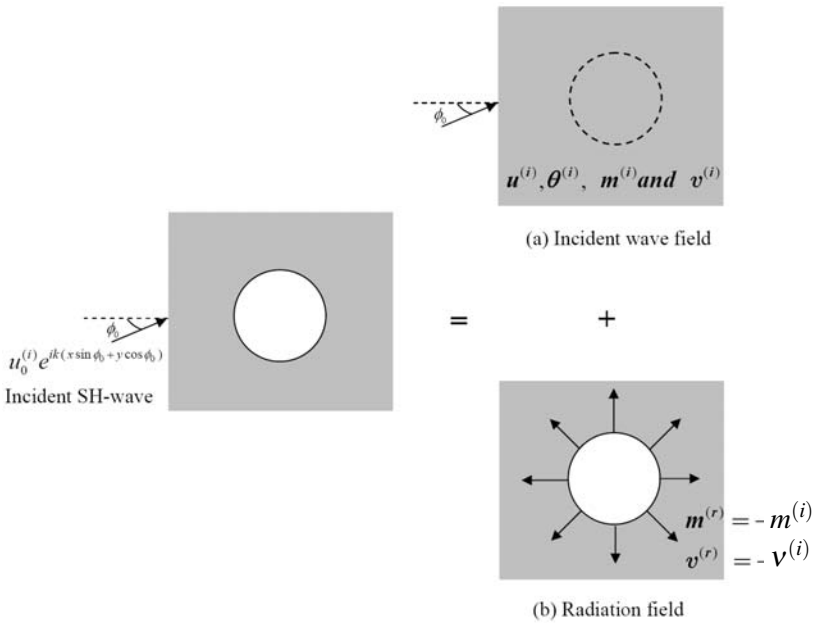

Figure 5: The decompositon of scattering problem into (a) incident wave field and (b) radition field

An incident flexural wave is represented by

$$u_0^{(i)} e^{ik(x\cos(\phi_0)+y\sin(\phi_0))} \tag{38}$$

where $u_0^{(i)}$ is the amplitude of incident wave, k is the wave number and ϕ_0 is the incident angle. Under the polar coordinate, the bending moment and effective shear force induced by the incident wave can be determined by substituting Eq. (38) into

Eqs.(15) and (16). By setting the amplitude of incident wave $u_0^{(i)} = 1$, the amplitude of moment produced by the incident wave is

$$M_0 = Dk^2 \tag{39}$$

The dynamic moment concentration factor (DMCF) at any field point x can be determined as

$$DMCF(x) = M_t(x)/M_0 \tag{40}$$

6 Numerical results and discussions

Scattering problems of flexural wave in thin plate with multiple holes are solved and dynamic moment concentration factors (DMCFs) around the circular holes are determined by using the present method. For the cases of small wave number, the same plate problem is independently solved by using FEM (the ABAQUS software) for comparison. In all cases, the inner boundary is subject to the free boundary condition and the thickness of plate is 0.002m. The triangular general-purpose shell element, S3, of ABAQUS was used to model the plate problem. Although the thickness of the plate is 0.002 m, these elements do not suffer from transverse shear locking according to the theoretical manual of ABAQUS.

Case 1: An infinite plate with one hole [Pao and Mow (1972); Kung (1964); Norris and Vemula (1995); Gao, Wang and Ma (2001); Gao, Wang, Zhang and Ma (2005)]

An infinite plate with one hole (radius a = $1m$) subject to the incident flexural wave with $\phi_0 = 0$ is considered as shown in Figure 6. Since the analytical solution of this problem is available, convergence analysis is firstly conducted. Figure 7 shows the DMCF on the circular boundary, at $\pi/2$, versus the dimensionless wave number by using different number of terms of Fourier series. From the convergence analysis, the required number of terms to approach the analytical solution increase as the incident wave number becomes larger. Results of the present method match well with those of analytical solution when the number of terms of Fourier series amounts to M = 10. The convergence analysis indicates that results using Fourier series with M = 2 match well with the analytical solution when the wave number is 0.005. For the case of the higher wave number k = 3.0, more number of terms are required to the same extent of convergence, which shows the consistency with the results presented by Figure 7.

In the limit of zero wave number [Pao and Mow (1972); Kung (1964)] like k = 0.005, the excitation of incident wave is equivalent to the loading with static moment $M_{xx} = M_0$ and $M_{yy} = \nu M_0$ at the four sides of a plate. Accordingly, a $16m \times 16m$ plate with one hole subject to static bending moments, $M_{xx} = 1.0$ and

$M_{yy} = 0.3$ at the four sides was considered. For this equivalent static case, 25567 triangle elements were used to generate the FEM model and Figure 8(a) shows the corresponding result of the normalized tangential bending moment around the hole. By using the present method, the unknown boundary densities of the plate are expressed in terms of Fourier series and the numerical result of DMCF around the hole using Fourier series terms (M = 10) is shown in Figure 8(b). The analytical solution [Pao and Mow (1972); Kung (1964)] is also shown in Figure 8(c) and good agreements are made after comparing with three different approaches stated above.

Figure 9 shows that the real and imaginary parts of DMCF on the circular boundary at $\pi/2$ versus the dimensionless wave number for various Poisson ratios by using the present method and the analytical solution [Pao and Mow (1972); Kung (1964)]. It indicates that both results match well and DMCF depends on the Poisson ratio of the plate as well as the incident wave number. For the dimensionless wave number ka=3.0, the real and imaginary parts of DMCF along the circular boundary is shown in Figures 10, which agrees with the result reported in Gao *et al*. [Gao, Wang, Zhang and Ma (2005)]. The value of DMCF is symmetrical to x-axis due to the incident wave with $\phi_0 = 0$. Table 1 lists dynamic moment concentration factors on the circular boundary ($\theta = \pi/2$) by using four approaches, dual reciprocity boundary element method [Gao, Wang, Zhang and Ma (2005)], boundary element method based on the dynamic fundamental solution [Gao, Wang and Ma (2001)], the present method and the analytical solution [Pao and Mow (1972); Kung (1964)], respectively. In addition to the required number of Fourier series terms to convergence, results of the present method are the same as the analytical solutions up to four digits. The present method is obviously superior to the BEM thanks to the semi-analytical procedure.

For the most part of scattering applications, it is interesting to measure the scattered field far away from the scatter. On the other hand, the asymptotic behavior or uniqueness of fundamental solutions or kernel functions is an important issue for the numerical computation. Therefore, we examine the behavior of the scattered response in the far field. The scattered far field amplitude $f(\theta)$ [Norris and Vemula (1995)] in our approach is defined as

$$f(\theta) = \lim_{\rho \to \infty} \sqrt{2\rho} \cdot u^{(r)}(\rho) \tag{41}$$

where $u^{(r)}$ is the out-of-plane elastic displacement of radiation field and ρ is the radius of the field point. In the computation, the radius of the field point is taken 90m because $f(\theta)$ converges a steady value when this radius is more than about 90m. Figure 11 shows a polar plot of the far field scattering amplitude for a circular hole in a 0.025m steel plate, solid line for ka = 1.0, dash line for ka = 0.5. Figure 12 presents the far field backscattered amplitude versus the dimensionless wave

number for an incident wave of unit amplitude, solid line for the hole, dash line for the rigid inclusion. The rigid inclusion means the clamped boundary condition around the circular boundary. As the dimensionless wave number becomes large, results of both cases approach the same value of one. The results for the hole show a local maximum near the small wave number and then increase with the wave number, which consists with with the results shown in Figure 11. The results match well with those of Norris and Vemula [Norris and Vemula (1995)]. It can be found that the amplitude for the radiation (or scattering) response in the far field is $O(\rho^{-1/2})$, which satisfy the radiation condition.

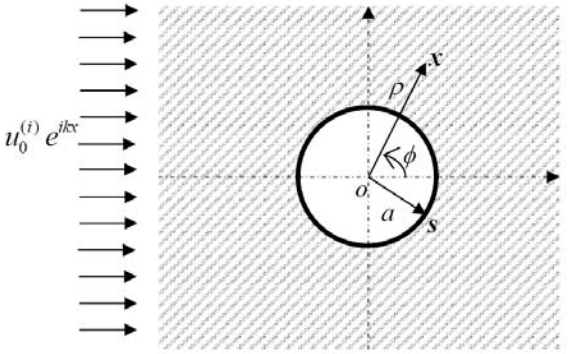

Figure 6: An infinite plate with one hole subject to an incident flexural wave

Table 1: Dynamic moment concentration factor on the circular boundary ($\theta = \pi/2$)

k	$f = 1 + r^*$	$f = 1 - r - r^*$	Ref **	Present method	Analytical solution
0.1	1.8285	1.8301	1.8360	1.8353(4)	1.8353(4)
0.5	1.6681	1.6692	1.6710	1.6616(6)	1.6616(6)
1.0	1.6452	1.6437	1.6420	1.5109(6)	1.5109(6)
2.0	1.6439	1.6458	1.6550	1.5894(8)	1.5894(8)
3.0	1.6475	1.6483	1.6500	1.5868(12)	1.5868(12)
5.0	1.6503	1.6509	1.6520	1.6305(14)	1.6305(14)

( ) denotes the required number of terms to converge to the steady result within four digits.

* refer to the results [Gao, Wang, Zhang and Ma (2005)]

** refer to the results [Gao, Wang and Ma (2001)]

Case 2: An infinite plate with two holes [Hu, Ma and Huang (1998)]

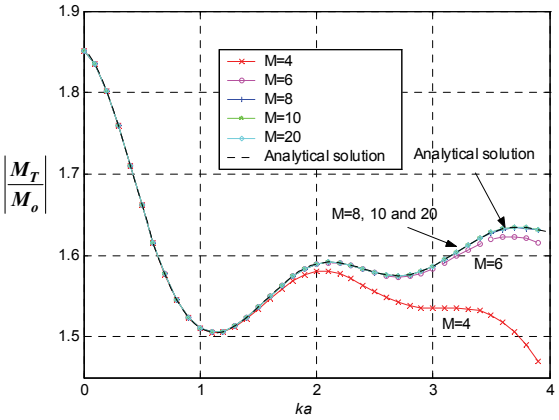

Figure 7: Dynamic moment concentration factor on the circular boundary ($\theta = \pi/2$) versus the dimensionless wave number by using different number of terms of Fourier series

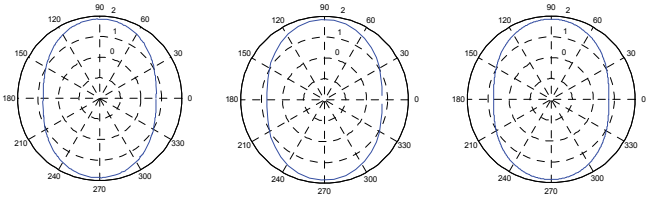

(a) FEM (ABAQUS, under equivalent static loading)

(b) Present method (M=10, *ka=0.005*)

(c) Analytical solution (*ka=0.005*)

Figure 8: Distribution of dynamic moment concentration factors on the circular boundary by using different methods, the present method, analytical solution and FEM

An infinite plate with two holes (radius $a = 1m$) subject to the incident flexural wave with $\phi_0 = 0$ is considered as shown in Figure 13, where L is the central distance of two holes. For the case of $L = 2.1m$, Figure 14 shows the DMCF on the upper circular boundary, at $-\pi/2$, versus the dimensionless wave number by using different number of Fourier series terms. From this convergence analysis, the results using fewer Fourier series terms show some peaks at *ka*=3.2, 4.6. Even so, the convergence is fast achieved when the number of Fourier series terms M amounts to twenty. Values of wave number corresponding to those peaks are found to be equal

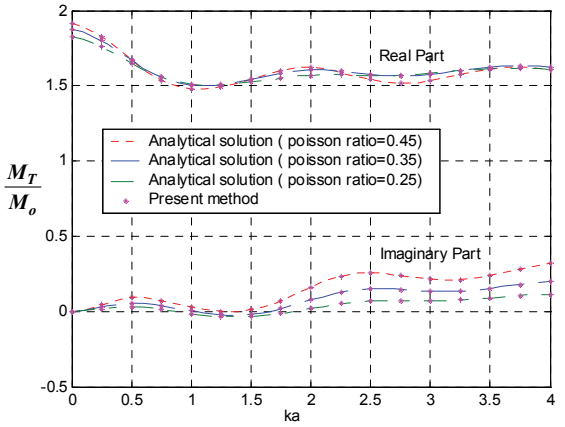

Figure 9: The real and imaginary parts of DMCF on the circular boundary ($\theta = \pi/2$) versus the dimensionless wave number for different Poisson ratios

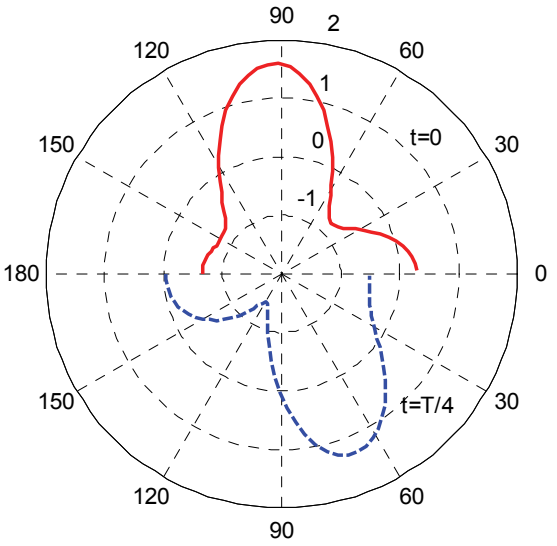

Figure 10: Distribution of DMCF (M_T/M_0) on the circular boundary, solid line (real part) for t = 0 for, dash line (imaginary part) for $t = T/4$ (ka = 3.0)

to the true eigenvalues of the clamped circular plate with a radius equaling to that of the hole, i.e. 3.196, 4.610 [Leissa (1969)]. Actually they are the so-called fictitious frequencies of the external problem. It demonstrates that the increasing number of

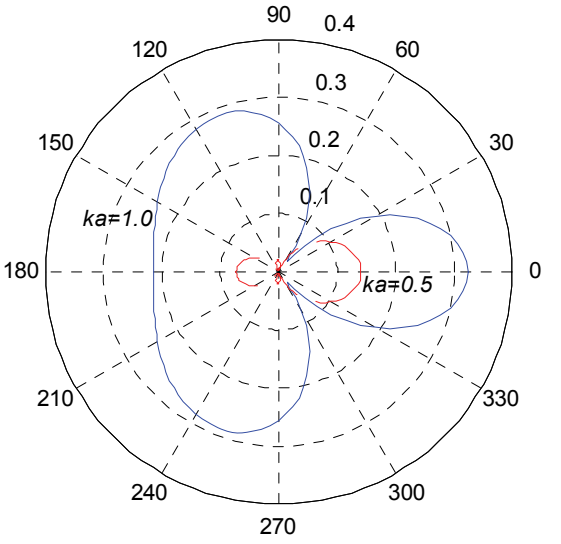

Figure 11: A polar plot of the far field scattering amplitude for a circular hole in a 0.025m steel plate, solid line for $ka = 1.0$, dash line for $ka = 0.5$

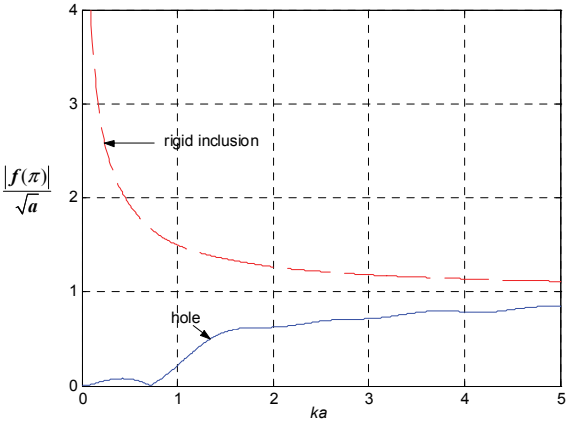

Figure 12: The magnitude of the backscattered far field flexural response for an incident wave of unit amplitude. The surrounding plate is steel of thickness 0.025m, solid line for hole, dash line for rigid inclusion

Fourier series terms can suppress the appearance of fictitious frequencies.

For comparison with the proposed method, we consider a $16m \times 22m$ plate with two holes (L = 2.1m) subject to static bending moments, $M_{xx} = 1.0$ and $M_{yy} = 0.3$

at the four sides. For this case, 49024 triangle elements were used to generate the FEM model and the corresponding result of the normalized tangential bending moment around the hole is shown in Figure 15(a). The result of the present method for k = 0.005 is also shown in Figure 15(b) and good agreements are made after comparison. It indicates that the maximum DMCF is larger than that of one hole shown in Figure (8) due to two close holes in this case.

For the case of $L = 4.0m$, Figure 16 shows the DMCF on the upper circular boundary, at $-\pi/2$, versus the dimensionless wave number by using different number of terms of Fourier series. Instead of peak appeared in Figure 14, the result of convergence is similar to that of the case with one hole shown in Figure 7 due to two holes separated apparently.

For the dimensionless incident wave number ka=0.2 with the central distance between two holes L=2.1a, Figure 17 shows the distribution of the amplitude of DMCF on the circular boundary, solid line for one hole and dash line for the upper one of two holes. The DMCF of two holes is apparently larger than that of one hole when two holes are close each other.

Figure 18 shows the DMCF at the upper circular edge $(-\pi/2)$ versus the dimensionless central distance under different incident wave number, where the dot line denotes the corresponding results for one hole case. It indicates that when the central distance between two holes gradually increases, the results for the case of two holes approach that of the case with one hole. For the case of k= 2.0, oscillation behavior of DMCF is observed as the central distance of two holes varies. It is not found for the cases with the small wave number such as ka=0.1, 0.2 and 0.5. Furthermore, we zoom in the data of ka=0.1 at upper right corner (in the range of 1.834 to 1.838 for $|M_T/M_0|$). Then, it is refound that the oscillation behavior of DMCF with a period $2\pi/k$ versus L/a for all wave numbers appears, which was not found in Hu *et al.* [Hu, Ma and Huang (1998)]

7 Conclusions

A semi-analytical approach to solve the scattering problem of flexural waves and to determine dynamic moment concentration factors in an infinite thin plate with multiple circular holes was proposed. The radiation field was determined by employing the null-field integral formulation in conjunction with degenerate kernels, tensor transformation and Fourier series. All the improper integrals in the null-field integral formulation were avoided by using the degenerate kernels and were easily calculated through the series sum. For the general exterior case, the rotated degenerate kernels have been derived in the adaptive observer system. Once the Fourier coefficients of boundary densities have been determined, the flexural wave

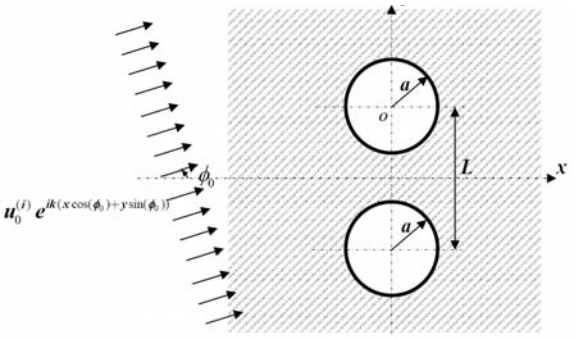

Figure 13: An infinite plate with two holes subject to an incident flexural wave with an incident angle ϕ_0

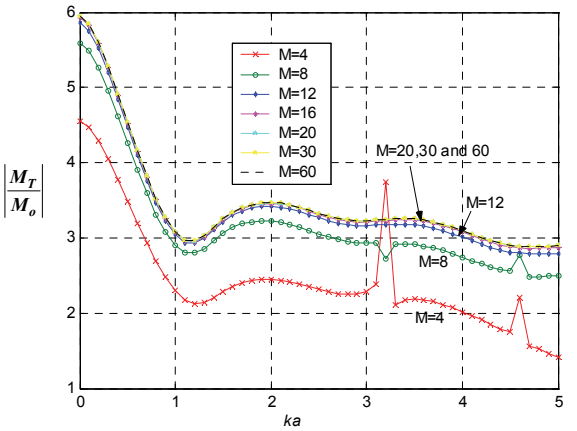

Figure 14: DMCF on the upper circular boundary ($\theta = -\pi/2$) versus the dimensionless wave number by using different number of terms of Fourier series (L/a= 2.1)

scattering field and dynamic moment concentrations can be obtained by using the boundary integral equations for domain points in conjunction with general rotated degenerate kernels. For an infinite plate with one hole, good agreement between the results of the present method and those of analytical solution is observed. For the cases of small wave number, the present results for a plate with one or multiple circular holes are well compared with the static case of finite element method (FEM) using ABAQUS. Convergence rate depends on two parameters of the incident wave number and the central distance between two holes. Numerical results

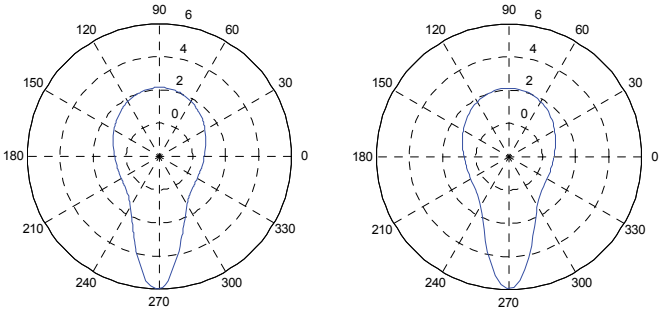

(a) FEM (ABAQUS, under equivalent static loading) (b) Present method (M=20, ka=0.005)

Figure 15: Distribution of DMCF on the upper circular boundary by using different methods, the present method and FEM (L/a= 2.1)

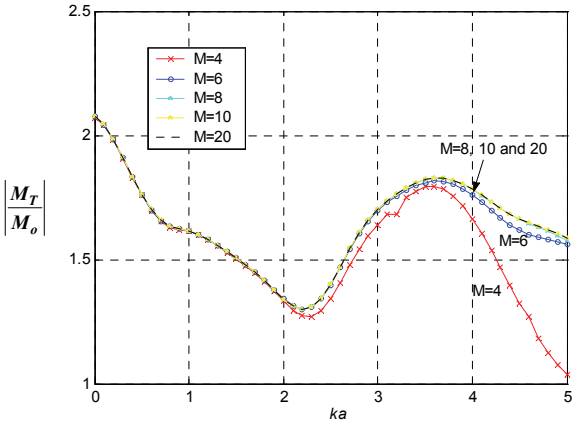

Figure 16: DMCF on the upper circular boundary ($\theta = -\pi/2$) versus the dimensionless wave number by using different number of terms of Fourier series (L/a= 4.0)

indicate that the DMCF of two holes is apparently larger than that of one hole when two holes are close to each other. Fictitious frequency of external problem can be suppressed by using the more number of Fourier series terms. The effect of the central distance on DMCF has been studied by using the present method and indicates a regular variation of DMCF as the central distance of two holes increases. As can be seen from the numerical results, the present method provides a semi-analytical solution for dynamic moment concentration factors in infinite thin plates with mul-

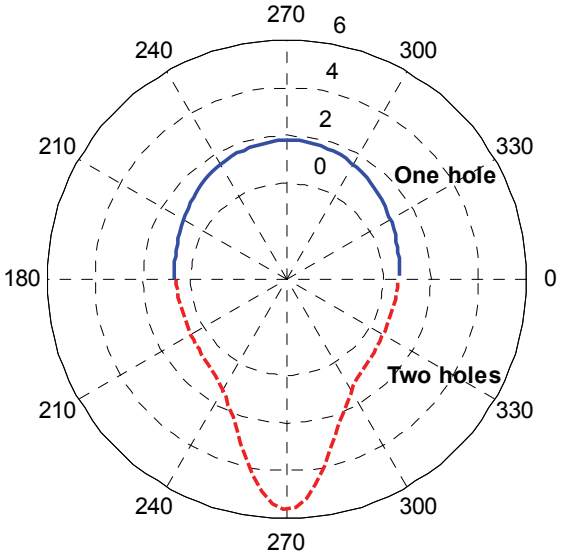

Figure 17: Distribution of DMCF $|M_T/M_0|$ on the circular boundary, solid line for one hole and dash line for the upper one of two holes ($L = 2.1a$, $ka = 0.2$)

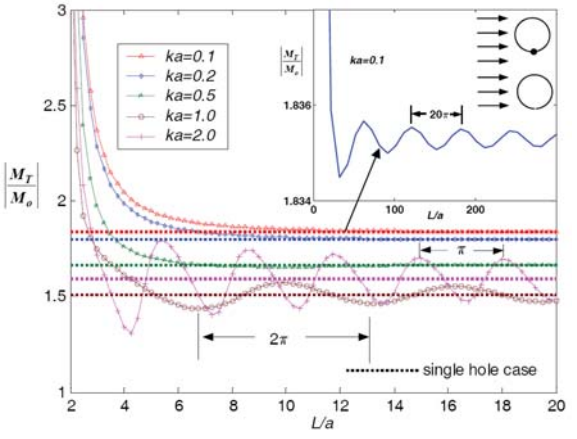

Figure 18: DMSF $|M_T/M_0|$ on the circular boundary ($\theta = -\pi/2$) versus the dimensionless central distance of two holes for different wave number under the incident wave with $\phi_0 = 0$

tiple circular holes subject to the incident flexural wave, since its analytical solution is not yet available.

Acknowledgement: Financial support from the National Science Concil under the Grant No. NSC-97-2211-E-157-006 for China Institute of Technology and NSC-97-2211-E-019-015-MY3 and MDE-CMBB-97-G-A-601 for Taiwan Ocean University is gratefully acknowledged.

References

Beskos, D. E. (1997): Boundary element methods in dynamic analysis: part $\not{\iota}^{o}$ (1986-1996). *Applied Mechanics Reviews ASME,* vol. 50, no.3, pp. 149-197.

Chandrasekhar, B.; Rao, S. M. (2007): Acoustic Scattering from Fluid Bodies of Arbitrary Shape. *CMES: Computer Modeling in Engineering and Sciences*, vol. 21, No. 1, pp. 67-80.

Chandrasekhar, B. (2008): Node based Method of Moments Solution to Combined Layer Formulation of Acoustic Scattering. *CMES: Computer Modeling in Engineering and Sciences*, vol. 33, No. 3, pp. 243-267.

Chen, H. B.; Fu, D. J.; Zhang, P. Q. (2007): An Investigation of Wave Propagation with High Wave Numbers via the Regularized LBIEM. *CMES: Computer Modeling in Engineering and Sciences*, vol. 20, No. 2, pp. 85-98.

Chen, J. T.; Hong, H. K. (1999): Review of dual boundary element methods with emphasis on hypersingular integrals and divergent series. *Applied Mechanics Reviews ASME,* vol. 52, no. 1, pp. 17-33.

Chen, J. T.; Shen, W. C.; Chen, P. Y. (2006a): Analysis of circular torsion bar with circular holes using null-field approach. *CMES: Computer Modeling in Engineering & Science*, vol. 12, pp. 109-119.

Chen, J. T.; Hsiao, C. C.; Leu, S. Y. (2006b): Null-field integral equation approach for plate problems with circular holes. *Transactions of the ASME Journal of Applied Mechanics,* vol. 73, pp. 679-693.

Chen, J. T.; Chen, C. T.; Chen, P. Y.; Chen, I. L. (2007): A semi-analytical approach for radiation and scattering problems with circular boundaries. *Computer Methods in Applied Mechanics and Engineering,* vol. 196, pp. 2751-2764.

Chen, J. T.; Ke, J. N. (2008): Derivation of anti-plane dynamic green's function for several circular inclusions with imperfect interfaces. *CMES: Computer Modeling in Engineering & Science*, vol. 29, pp. 111-135.

Gao, S. W.; Wang, B. L.; Ma, X. R. (2001): Scattering of elastic wave and dynamic stress concentrations in thin plate with a circular hole. *Engineering Mechanics,* vol. 18, no. 2, pp. 14-20.

Gao, S. W.; Wang, Y. S.; Zhang, Z. M.; Ma, X. R. (2005): Dual reciprocity boundary element method for flexural waves in thin plate with cutout. *Applied*

Mathematics and Mechanics, vol. 26, no. 12, pp. 1564-1573.

Gradshteyn, I. S.; Ryzhik, I. M. (1996): Table of integrals, series, and products. 5th edition, Academic Press.

Hayir, A., Bakirtas, I. (2004): A note on plate having a circular cavity excited by plane harmonic SH waves. *Journal of Sound and Vibration,* vol. 271, pp. 241–255.

Hu, C.; Ma, X. R.; Huang, W. H. (1998): Dynamic stress concentrations in thin plates with two circular cutouts. *Acta Mechanica Sinica*, vol. 30, no. 5, pp. 587–596.

Hu, C.; Fang, X.; Huang, W. (2007): Multiple scattering of flexural waves in a semi-infinite thin plate with a cutout. *International Journal of Solids and Structures,* vol. 44, pp. 436-446.

Hutchinson, J. R. (1991): Analysis of plates and shells by boundary collocation. In: Beskos DE (ed) *Boundary Elements Analysis of Plates and Shells*. Springer Berlin, pp. 314-368.

Kitahara, M. (1985): Boundary integral equation methods in eigenvalue problems of elastodynamics and thin plates. Elsevier, Amsterdam.

Kobayashi, S.; Nishimura, N. (1981): Transient Stress Analysis of Tunnels and Caverns of Arbitrary Shape Due to Traveling Waves. in: *Developments in Boundary Element Methods-II* , Banerjee, P . K., and Shaw, R. P., eds., Applied Science, London, pp. 177-210.

Kress, R. (1989): Linear integral equations, Springer-Verlag, Berlin.

Kung, George C. S. (1964): Dynamical stress concentration in an elastic plate. M.S. Thesis, Cornell University, Ithaca, NY.

Leissa, W. (1969): Vibration of plates. NASA SP-160.

Lin, D.; Gai, B.; Tao, G. (1982): Applications of the method of complex functions to dynamic stress concentrations. *Wave Motion,* vol. 4, pp. 293-304.

Martin, P. A. (2006): Multiple scattering interaction of time-harmonic wave with N obstacles. Cambridge University Press, UK.

Nishimura, G.; Jimbo, Y. (1955): A dynamical problem of stress concentration. *Journal of the Faculty of Engineering*, University of Tokyo, Japan, vol. 24, pp. 101.

Norris, A. N.; Vemula, C. (1995): Scattering of flexural waves on thin plates. *Journal of Sound and Vibration,* vol. 181, pp. 115-125.

Pao, Y. H.; Mow, C. C. (1972): Diffraction of elastic waves and dynamics stress concentration. Crane, New York.

Pao, Y. H. (1962): Dynamical stress concentration in an elastic plate. *Transactions*

of the ASME Journal of Applied Mechanics, June, pp. 299-305.

Squire, V. A.; Dixon, T. W. (2000): Scattering of flexural waves from a coated cylindrical anomaly in a thin plate. *Journal of Sound and Vibration*, vol. 236, no. 2, pp. 367-373.

Tanaka, M.; Sladek, V.; Sladek, J. (1994): Regularization techniques applied to boundary element methods. *Applied Mechanics Reviews,* vol. 47, pp. 457-499.

Appendix I: Degenerate kernels

$$U^j(x,s) = \sum_{m=0}^{\infty} f_j cos(m(\theta-\phi_i)), \quad j=1,2$$

where

$$f_1 = \frac{1}{8k^2D}\varepsilon_m\{J_m(k\rho)[Y_m(kR) - iJ_m(kR)] + \frac{2}{\pi}I_m(k\rho)K_m(kR)\}$$

$$f_2 = \frac{1}{8k^2D}\varepsilon_m\{J_m(kR)[Y_m(k\rho) - iJ_m(k\rho)] + \frac{2}{\pi}I_m(kR)K_m(k\rho)\}$$

$$\Theta^j(x,s) = \frac{\partial U^j(x,s)}{\partial R} = \sum_{m=0}^{\infty} g_j cos(m(\theta-\phi)), \quad j=1,2$$

where

$$g_1 = \frac{1}{8kD}\varepsilon_m\{J_m(k\rho)[Y'_m(kR) - iJ'_m(kR)] + \frac{2}{\pi}I_m(k\rho)K'_m(kR)\}$$

$$g_2 = \frac{1}{8kD}\varepsilon_m\{J'_m(kR)[Y_m(k\rho) - iJ_m(k\rho)] + \frac{2}{\pi}I'_m(kR)K_m(k\rho)\}$$

where

$$\varepsilon_m = \begin{cases} 1 & m=0 \\ 2 & m\neq 0 \end{cases},$$

the superscript j (1 or 2) denotes the interior domain (*i.e.* $\rho < R$, j =1) and exterior domain (*i.e.* $\rho > R$, j =2), respectively.

$$M^j(x,s) = \sum_{m=0}^{\infty} p_j \cos(m(\theta-\phi_i)), \quad j=1,2$$

where

$$p_1 = -\frac{1}{8k^2}\varepsilon_m\{J_m(k\rho)[\alpha_m^Y(kR) - i\alpha_m^J(kR)] + \frac{2}{\pi}I_m(k\rho)\alpha_m^K(kR)\}$$

$$p_2 = -\frac{1}{8k^2}\varepsilon_m\{\alpha_m^J(kR)[Y_m(k\rho) - iJ_m(k\rho)] + \frac{2}{\pi}\alpha_m^I(kR)K_m(k\rho)\}$$

$$\alpha_m^Y(kR) = k^2 Y_m''(kR) + \nu\left[\frac{k}{R}Y_m'(kR) - \frac{m^2}{R^2}Y_m(kR)\right]$$

$$\alpha_m^J(kR) = k^2 J_m''(kR) + \nu\left[\frac{k}{R}J_m'(kR) - \frac{m^2}{R^2}J_m(kR)\right]$$

$$\alpha_m^K(kR) = k^2 K_m''(kR) + \nu\left[\frac{k}{R}K_m'(kR) - \frac{m^2}{R^2}K_m(kR)\right]$$

$$\alpha_m^I(kR) = k^2 I_m''(kR) + \nu\left[\frac{k}{R}I_m'(kR) - \frac{m^2}{R^2}I_m(kR)\right]$$

$$V^j(x,s) = \sum_{m=0}^{\infty} q_j cos(m(\theta - \phi_i)), \quad j = 1,2$$

where

$$q_1 = -\frac{1}{8k^2}\varepsilon_m\{J_m(k\rho)[\beta_m^Y(kR) - i\beta_m^J(kR)] + \frac{2}{\pi}I_m(k\rho)\beta_m^K(kR)\}$$

$$q_2 = -\frac{1}{8k^2}\varepsilon_m\{\beta_m^J(kR)[Y_m(k\rho) - iJ_m(k\rho)] + \frac{2}{\pi}\beta_m^I(kR)K_m(k\rho)\}$$

$$\beta_m^Y(kR) = k^3 Y_m'''(kR) + \frac{k^2}{R}Y_m''(kR) - \frac{k}{R^2}\left[1 + (2-\nu)m^2\right]Y_m'(kR) + \left[\frac{(3-\nu)m^2}{R^3}\right]Y_m(kR)$$

$$\beta_m^J(kR) = k^3 J_m'''(kR) + \frac{k^2}{R}J_m''(kR) - \frac{k}{R^2}\left[1 + (2-\nu)m^2\right]J_m'(kR) + \left[\frac{(3-\nu)m^2}{R^3}\right]J_m(kR)$$

$$\beta_m^K(kR) = k^3 K_m'''(kR) + \frac{k^2}{R}K_m''(kR) - \frac{k}{R^2}\left[1 + (2-\nu)m^2\right]K_m'(kR) + \left[\frac{(3-\nu)m^2}{R^3}\right]K_m(kR)$$

$$\beta_m^I(kR) = k^3 I_m'''(kR) + \frac{k^2}{R} I_m''(kR) - \frac{k}{R^2}\left[1+(2-\nu)m^2\right] I_m'(kR) + \left[\frac{(3-\nu)m^2}{R^3}\right] I_m(kR)$$

where

$$\varepsilon_m = \begin{cases} 1 & m = 0 \\ 2 & m \neq 0 \end{cases},$$

the superscript j (1 or 2) denotes the interior domain (*i.e.* $\rho < R$, j =1) and exterior domain (*i.e.* $\rho > R$, j =2), respectively.

Appendix II: Degenerate kernels with respect to the adaptive observer system

The expressions for U_θ, Θ_θ, M_θ and V_θ can be obtained by replacing L in Eq.(A1) by U, Θ, M and V, and replacing h in Eq.(A1) by f, g, p and q, respectively. The definition of U, Θ, M, V, f, g, p and q can be seen in the Appendix I.

$$L_\theta^j(x,s) = \sum_{m=0}^{\infty} c_1 h_j' cos(m(\theta-\phi_i)) + s_0 h_j sin(m(\theta-\phi_i)), \quad j = 1,2 \tag{A1}$$

where $c_1 = \cos(\delta_i)$, $s_0 = \left(\frac{m}{\rho_i}\right) sin(\delta_i)$ and $\delta_i = \phi_c - \phi_i$. The expressions for U_m, Θ_m, M_m and V_m can be obtained by replacing L in Eq.(A2) by U, Θ, M and V, and replacing h in Eq.(A2) by f, g, p and q, respectively

$$L_m^j(x,s) = \sum_{m=0}^{\infty} [mc_0 h_j + mc_1 h_j' + mc_2 h_j''] \cos(m(\theta-\phi_i)) + [ms_0 h_j + ms_1 h_j'] \sin(m(\theta-\phi_i)), \quad j = 1,2 \tag{A2}$$

where

$$mc_0 = -\left(\frac{m^2}{2\rho_i^2}\right)(1+\nu+(-1+\nu)cos(2\delta_i)),$$

$$mc_1 = \left(\frac{1}{2\rho_i}\right)(1+\nu+(-1+\nu)cos(2\delta_i)),$$

$$mc_2 = \left(\frac{1}{2}\right)(1+\nu+(1-\nu)cos(2\delta_i)),$$

$$ms_0 = \left(\frac{m}{\rho_i^2}\right)(-1+\nu)sin(2\delta_i),$$

$$ms_1 = \left(\frac{m}{\rho_i}\right)(1-\nu)sin(2\delta_i),$$

the superscript j (1 or 2) denotes the interior domain (*i.e.* $\rho < R$, $j = 1$) and exterior domain (*i.e.* $\rho > R$, $j = 2$), respectively.